Surface Tension Dynamics in 3D-Printed Components: Exploring Materials, Manufacturing Technologies and Wetting Behavior

Csilla Agócs[1], Muammel M. Hanon[2*] and László Zsidai[3]

[1] Mechanical Engineering Doctoral School, Hungarian University of Agriculture and Life Sciences, Páter Károly u. 1, 2100 Gödöllő, Hungary; agocs.csilla@phd.uni-mate.hu

[2] Baquba Technical Institute, Middle Technical University (MTU), Muasker Al-Rashid Street, 10074 Baghdad, Iraq; muammel.m.hanon@mtu.edu.iq

[3] Department of Materials Science and Mechanical Processes, Hungarian University of Agriculture and Life Sciences, Páter Károly u. 1, 2100 Gödöllő, Hungary; zsidai.laszlo@uni-mate.hu

Abstract: This study investigates the complex correlation between surface tension and the existing 3D-printed components, along with their manufacturing technologies to provide potential directions for understanding surface properties in 3D printing. The research focuses on the wetting and surface tensions of different polymeric materials pairs, with different 3D printed materials, such as PLA, bronze powder filled PLA, ABS, gray epoxy resin and white epoxy resin, with diiodomethane and water. The study employs advanced measurement techniques for systematic investigations of surface tension properties. Because of this, Krüss DSA30 is the most common surface tension measurement apparatus, specialized in the detection of drop shapes. In this work, the effect of 3D printing technology on surface tension dynamics was explored, using digital light processing (DLP) and fused deposition modeling (FDM) to develop insights into how strength characteristics are governed by the processes used to fabricate materials. The resulting data showed varying levels of surface free energy across a range of materials, suggesting that white and gray epoxy resins may offer superior frictional properties coupled with elevated adhesion. Concisely, this work offers enhancing the functionality and performance of 3D-printed components across diverse applications in different sectors by establishing the foundation for optimized surface tension.

Keywords: surface tension measurement; contact angle measurement; additive manufacturing; wetting behavior; DLP; FDM

1 Introduction

Surface tension and contact angles come from the intermolecular forces. The challenge is to understand how these short-range forces translate into macroscopically observable behavior of liquids [1] [2]. Recently, the surface properties of 3D-printed elements have gained a notable attention due to their critical role in influencing the effectiveness of manufactured goods across various sectors [3-6]. The 3D printed components behavior significantly influences the surface tension features at the solid-liquid interface which indicates the prominence of comprehending its characteristics. The unique molecular forces occurring at the interface are controlled by the inherent properties of liquids owing to the surface tension [7] [8]. To express the surface tension (γ) mathematically, it is the difference in free energy per unit change of surface area (ΔAs) with preserving a constant volume [9] [10]:

$$\gamma = \left(\frac{\partial G}{\partial A_S}\right)_{p,T} \tag{1}$$

The importance of this concept lies in the comprehension of how interactions occur between 3D-printed components and surrounding liquids and solids, affecting wetting behavior and adhesion. However, wetting, which is closely connected to surface tension, is defined by how a solid surface is adhered to by a liquid and is influenced by the balance between the surface tensions of the liquid-solid (γ_{LS}), liquid-vapor (γ_{LV}), and solid-vapor (γ_{SV}) interfaces [11]:

$$\cos\Theta = \frac{(\gamma_{SV}-\gamma_{LS})}{\gamma_{LV}} \tag{2}$$

In this context, the contact angle, denoted by Θ, is used, where greater wetting is signified by a smaller contact angle, and a 0° angle indicates perfect wetting. Conversely, an angle of 180° implies that there is no adhesion between the liquid and solid phases (refer to Figure 1). The contact angle, therefore, is regarded as a critical indicator of wetting behavior and adhesion properties at the liquid-solid interface [12].

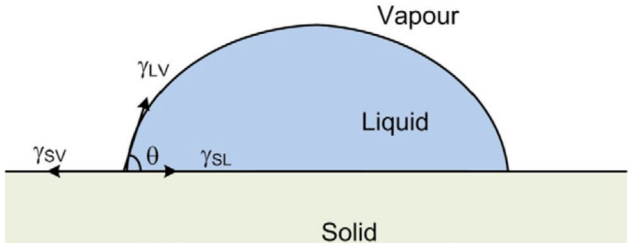

Figure 1
Illustration of Young's conceptualization of the force equilibrium at a three-phase contact line, involving a droplet, its vapor, and a solid surface. In this traditional representation, the three mechanical surface tensions (γ_{SV}, γ_{SL}, and γ_{LV}) are balanced in the direction parallel to the solid surface [13]

Equally vital for 3D-printed components is the understanding of the pressure balance within the liquid-solid interface, given the three-dimensional characteristics of the interface [14, 15]. The forces contributing to tension at the interface are demonstrated by an integral equation [16]

$$\int_{\alpha}^{\beta}(P - P_T)\,dz = \frac{F}{l} = \gamma \tag{3}$$

The force (F) at the interface is demonstrated by this integral equation to arise from the difference between the overall pressure (P) and the tangential pressure (P_T), z is the spatial coordinate normal to the interface. The integral appears in the equation because the pressure difference ($P - P_T$) may vary along the z-direction, across the interface. The integration sums this spatial variation of the pressure difference between the limits α and β, providing the total surface force. These forces significantly impact wetting and adhesion properties [17]. These surface tension phenomena, demand that one explain within the paradigm of 3D-printed parts, factoring in the space of the manufacturing mechanisms applied. The most frequent 3D printing technologies are fused deposition modeling (FDM) and digital light processing (DLP), which contribute to a variety of surface properties [18-23].

A review of both experimental and theoretical previous works in this area is required to gain a more in-depth understanding of the surface tension characteristics of the 3D-printed parts. The surface tension found in studies have been addressed in different ways, providing perspectives and views applicable to different use. For example, Sanatgar et al. Garg et al. (2017) investigated three-dimensional (3D) printing as a novel technique for the deposition of polymers onto synthetic textiles, intended on being a more flexible, resource efficient, and cost effective method of textile functionalization compared to classic printing methods [24]. The adhesion of polymer and nanocomposite layers onto textile fabrics whilst varying 3D printing parameters, fabric type and filler type was the main focus of the study, which were all performed using fused deposition modeling (FDM) technology. The study highlighted the need for an integrated production process for smart textile development that saves water, energy, and chemicals, as well as minimization of waste and improvement of both ecological footprint and productivity. The results showed that different 3D printing variable conditions have a very strong impact on the adhesion forces as well as PLA and its composites show high adhesion on PLA fabrics. Huang et al. (2021) studied droplet deposition 3D printing for metal parts in space and emphasized how the effect of gravity on droplet spreading and solidification, makes ground-based simulation impossible [25]. The asymmetrical dynamics and solidification process of molten metal droplets hitting vertical substrates were investigated in detail in this study using numerical simulations and experiments. Gravity affected spreading, retraction and the shape of the solidification, and some key parameters like impact velocity and temperatures also played a role by affecting the undesired solidification shape. Also, Özenç et al. (2022) investigated how additive manufacturing can be used to create smaller sub-parts to circumvent the size limitation associated with traditional additive

manufacturing [26]. The study involved ASTMD 950-3 standard test specimens that were made out of polylactic acid (PLA) and acrylonitrile butadiene styrene (ABS) polymers bonded with the cyanoacrylate/epoxy mixture hybrid adhesive. On testing for impact strength using Izod tests, ABS parts showed higher impact strength as compared to PLA and 0.3 mm layer thickness was found to have the highest impact strength for ABS.

The study of surface free energy is of paramount importance in the application of polymers to frictional machine components, especially in terms of adhesive adhesion, which can be characterized by surface energy. Adhesive adhesion not only influences the degree of friction and wear, but also provides valuable information about the process of material transfer (transfer film) between polymers. In addition, it plays a significant role in the phenomenon of stick-slip, which is one of the most important challenges in industrial friction systems [27].

The influence of powder deterioration on the stability of a molten pool in a laser beam powder bed fusion (LB-PBF) process and its consequences for the physical properties of the alloy, porosity of 3D-printed components, and their mechanical properties is investigated in a study by Skalon et al. (2021) [28]. Ti6Al4V (15 μm-45 μm) serves as the base material in both fresh and degraded forms (reused 12 times), with alloy degradation analyzed through changes in particle shape, size distribution, chemical composition, surface tension, density, and viscosity. The study employs 3D printing singular lines to examine the molten pool's behavior at varying powder bed depths, revealing that powder degradation destabilizes the molten metal pool, impacting mechanical properties and facilitating localized lack of fusion between concurrent layers. Electromagnetic levitation (EML) measures surface tension and melt density, finding marginal or no impact on these properties due to increased oxygen content, with observed differences in the temperature dependence of surface tension. Further, Gao et al. (2021) introduced a programmable 3D printing method for magnetically driven micro soft robots, focusing on surface tension-based control of liquid printing material [29]. This involved making use of a high-performance surfactant to stabilize the silicone's structure, in addition to pre-printed auxiliary lines of ultraviolet curing adhesive that allowed for clear definition and retention of the silicone's form. Micro soft robots were printed with specific 2D (two-dimensional) structure through a reproducible silicone 3D printing process involving silicone with and without neodymium-iron-boron powder. In motion experiments, the viability of different driving modes was verified, and the motion performance of the microrobots was studied with respect to changes in printing and magnetically driven parameters. Moreover, Chan et al. (2023) studied 3D-printed textile fabrics with self-cleaning characteristics, an important aspect of the environment since they can provide water- and energy-saving and economical laundry [30]. As woven fabrics could be easily treated by traditional chemical coating methods, the study focused on the 3D-printed fabrics and its problems. The study derived a linear regression model correlating secondary 3D printing parameters (infill rate, flow rate, printing temperature, printing speed,

and printing acceleration) with self-cleaning properties of TPU fabric, of which flow rate was highlighted as the most significant parameter affecting the wettability of TPU fabric. In a study by Kalkandelen et al., the calcium phosphates were partly mixed with gelatin solutions and printed using a modified 3D printing machine, which allowed the researchers to analyze the influence of the printing parameters – temperature, viscosity, and surface tension of gelatin solutions – on the scaffolds structuring [31]. Gelatin solutions at different concentrations (1, 3, 5, 10, 15, and 20 wt.%) and characterized, showing that both temperature and gelatin concentration were major contributors to viscosity. Specifically, 67% porosity, CAD models were produced and it was found that the ideal 3D printing parameters for gelatin including temperature (25-35 °C), viscosity (36-163 cP), surface tension (46-59 mN/m), and gelatin concentration (15 wt.%).

The surface tension of 3D-printed components is essential as per the above studies which provide an understanding of what influences surface tension and how important is it for diverse applications. However, there is still a need for more research that can investigate the broader interrelations between surface tension properties, 3D printing technologies, geometrical complexities, and material compositions. Application of common liquids, e.g. water and diiodomethane, on 3D-printed materials including ABS and PLA to measure their surface tension is important for determining the relative wettability and adhesion of those materials, which is critical for many applications including coatings, adhesives, and biomedical devices. The polymer substrate and its printing parameters affect surface energy differences, therefore surface-liquid interactions. Quantifying these properties enhances the reliability and broadens the applications of additive manufacturing technologies. This study aims to expand the knowledge base by examining the wetting behavior and surface tension of diverse 3D-printed polymeric material pairs, including PLA, ABS, gray epoxy resin, white epoxy resin, and PLA filled with bronze powder, exposed to diiodomethane and water. The findings offer a comprehensive understanding of how different materials and printing methods affect surface qualities, paving the way for optimizing 3D-printed components' performance and functionality in various applications.

2 Materials and Methods

2.1 Measurement of Surface Tension

Surface tension, a fundamental characteristic of liquid behavior, is a dynamic phenomenon wherein the liquid surface strives to minimize its energy by contracting. This behavior can be analogously compared to an elastic membrane subject to a bounding force. Consequently, a force of magnitude $\Delta F = \gamma \Delta l$ comes into play.

For liquids, surface tension closely corresponds to the surface free energy. The distinction between these two quantities is often negligible, a phenomenon particularly pertinent to liquid systems. This congruence, however, is restricted to the liquid realm, as free energy inherently manifests as a scalar, while surface tension, for instance in solid-liquid interactions, assumes tensor characteristics.

Surface tension, in an initial approximation, remains agnostic to surface geometry, primarily relying on the liquid's intrinsic quality, state, and its immediate medium interface. This thermodynamic parameter is inherently temperature-dependent, inversely proportional to temperature, and vanishing at the critical point. The phenomenon is conveniently described by the Eötvös formula [32]:

$$\gamma V^{\frac{2}{3}} = K(T - T_c) \tag{4}$$

Here, K represents the Eötvös constant, T_c symbolizes the critical temperature, and V denotes the molar volume of the liquid.

The surface tension value is profoundly affected by molecular interactions and becomes readily altered upon interfacial contamination. Several established techniques are employed to gauge surface tension. These methods encompass the utilization of capillary tubes, dripping, the tear-out method, and edge angle determination.

2.2 Edge Angle Determination and Wetting Phenomena

Upon the deposition of a liquid droplet onto a solid surface, two fundamental behaviors may be observed. The droplet can either spread out to conform to the solid surface at a specific angle, with the deformed droplet unable to attain a lens-like form due to the minimal deformation of the solid interface. In the former scenario, where droplet spreading occurs, it is referred to as film or perfect wetting, while the latter case corresponds to contact or partial wetting.

Young's equation (Equation 2) provides a framework for quantifying the edge angle Θ, colloquially referred to as the fit angle or contact angle. Notably, as the edge angle diminishes, it corresponds to greater solid-liquid adhesion, with perfect wetting being achieved at an angle of 0°. In principle, the edge angle can reach a value of 180°, indicative of a lack of interphase adhesion. Thus, the magnitude of the edge angle effectively characterizes the extent of solid-liquid adhesion.

In instances of film wetting, the heat of immersion is a critical indicator of the degree of adhesion between the solid and liquid phases. The variation in enthalpy between the solid-liquid and solid-vacuum interfaces can be measured with remarkable precision using microcalorimeters. Greater thermal effects signify stronger adhesion, and the degree of spreading can be assessed through the spread coefficient (S):

$$S \geq \gamma_{SV} - \gamma_{LV} - \gamma_{SL} \geq 0 \tag{5}$$

In cases of partial wettability, numerous edge angles with variable magnitudes can be specified. The number of edge angles is contingent upon whether the objective is to establish or eliminate solid-liquid contact. When a suitably-sized droplet is placed on a horizontally oriented flat plate and the plate is inclined, the droplet assumes an asymmetrical form, exhibiting a larger edge angle on the side inclined toward gravitational descent in comparison to the opposing side.

The leading edge angle is ascertained at the front edge (advancing contact angle - Θ_A), while the trailing edge angle is identified at the rear (Θ_R). The angular hysteresis, denoted as H_Θ, quantifies the discrepancy between the leading and trailing angles:

$$H_\Theta = \Theta_A - \Theta_R \tag{6}$$

Increasing H_Θ values signify amplified surface heterogeneity, whether due to chemical or geometric influences. Edge angle determination is facilitated through tangent editing or droplet build-up and removal techniques.

Tangent editing involves the introduction of a tangent to the droplet contour and the solid surface at the point of three-phase contact. The angle enclosed by these two tangents is recognized as the peripheral angle (Figure 2).

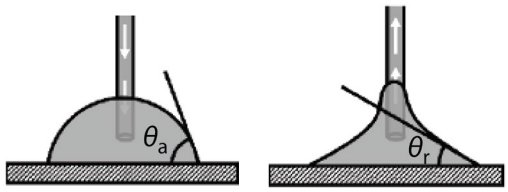

Figure 2
Determination of the advancing contact angle (Θ_A) and receding contact angle (Θ_R) using the drop deposition and drop withdrawal method [33]

Conversely, in the case of the droplet build-up and removal technique, solid-liquid contact is initially established during droplet formation, and subsequently, efforts are made to eliminate it as the liquid is extracted, as depicted in Figure 2.

When employing the seated drop methodology, it is imperative to mitigate the influence of gravity. This necessitates the examination of a minimal-mass drop, as gravitational forces have a negligible impact on droplet shape in this context.

The edge angle stipulated in Young's equation represents an equilibrium parameter. Thus, the presence of edge angle hysteresis indicates metastable states, characterized by values deviating from this equilibrium parameter. The equilibrium edge angle can be derived through the forward and backward edge angles:

$$\Theta = arc\ cos\left(\frac{cos\Theta_A + cos\Theta_R}{2}\right) \tag{7}$$

The edge angle is notably influenced by substances dissolved in the liquid, as molecules or ions of dissolved entities exhibit observable adsorption at the interfacial boundaries of the system (*SL*, *LV*, *SV*). This, in turn, influences the surface tension, thereby imparting changes to the edge angle.

To categorize surface adhesion properties, two distinct groups are identified based on their interaction with water. These groups encompass hydrophobic (water-repellent) and hydrophilic (water-attractive) surfaces. Hydrophobic surfaces display minimal energy, while hydrophilic surfaces exhibit elevated energy states. Consequently, surfaces with large edge angles, indicative of water-repellency, are associated with low-energy characteristics, while surfaces with small edge angles correlate with perfect wetting.

During the experimental investigations, a diverse set of material pairs were scrutinized with water and diiodomethane (CH_2I_2), including ABS, PLA, and PLA filled with bronze powder (FDM 3D-printed) as well as white epoxy resin and gray epoxy resin (DLP 3D-printed).

2.3 Sample Fabrication

Sample production was achieved through the utilization of 3D printers, operating on the principles of Fused Deposition Modeling (FDM) and Digital Light Processing (DLP). Specific printing parameters are provided in Table 1. The dimensions of all printed samples consistently measured 25 x 40 x 5 mm.

Table 1
3D printing parameters of materials investigated

Material	**ABS**	**PLA**	**PLA filled with bronze powder**	**White epoxy resin**	**Gray epoxy resin**
Parameter	**FDM printed**			**DLP printed**	
Printing temperature [°C]	250	195	195	25	25
Workbed temperature [°C]	60	25	25	-	-
Filling raster directions	45°/135°	45°/135°	45°/135°	-	-
Filling [%]	100%	100%	100%	100%	100%

2.4 Surface Tension Determination: Experimental Setup and Procedure

Surface tension measurements were conducted within the research facilities of the Colloid Chemistry Group, situated in the Department of Physical Chemistry and

Materials Science, Faculty of Chemical Engineering and Bioengineering at the Budapest University of Technology.

A Krüss DSA30 instrument (Figure 3), specializing in Drop Shape Analysis (DSA), served as the primary apparatus for these measurements. Prior to commencing each measurement, sample surfaces were diligently purged of any potential surface contaminants using isopropyl alcohol, followed by thorough rinsing with high-purity distilled water.

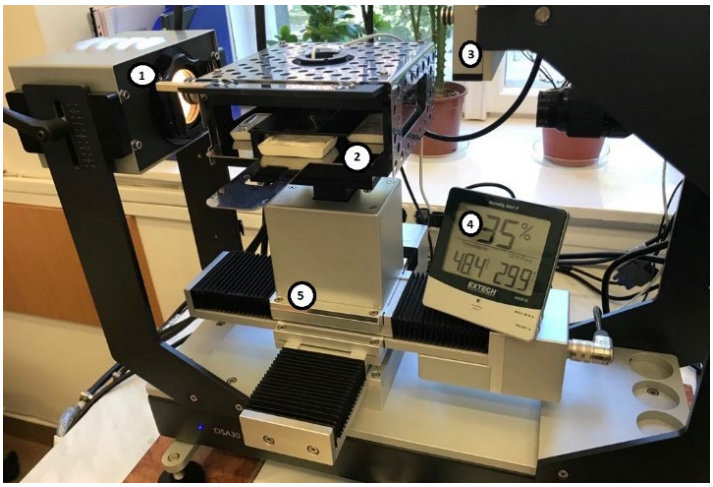

Figure 3
Krüss DSA30 device: 1 – light source, 2 – sample holder, 3 – drop dispenser, 4 – display (for temperature distribution, humidity), 5 – movable base

It is important to note, that surface tension properties are highly sensitive to temperature variations. As the measurements were performed at an ambient temperature of 25 °C, the results are applicable only within a narrow temperature range around this value [34]. Sample placement within the measurement device was executed using precision tweezers, ensuring a stable experimental environment. During the measurement process, a 10 µl liquid drop was dispensed onto the sample surface at a rate of 3 µl/s, facilitated by a needle with a diameter of 0.512 mm. The instrument was calibrated relative to the diameter of the needle, enabling precise determination of drop volume. A tilt angle of 2° was employed throughout the measurements. Each sample was subjected to a series of 3-6 parallel measurements, and the resulting data were aggregated by calculating the mean value for subsequent evaluation. When determining the droplets, the baseline was set subjectively, which could lead to a scatter in the values, therefore the calculations were performed with the Krüss Advance software, neglecting the smallest and largest values.

For these investigations, the selected measuring liquids included high-purity distilled water, diiodomethane, and cyclohexane. Notably, the high-purity distilled water used exhibited a measured resistance of R = 18.2 MΩcm, with the purification process carried out employing ion exchange resin and subsequent UV illumination.

Water has a high surface tension (~72 mN/m), making it sensitive to the polar nature of surface therefore it is excellent for highlighting hydrogen bonding and other polar interactions on surfaces. On the contrary, diiodomethane has a lower surface tension (~50 mN/m) and does not participate in hydrogen bonding, it is sensitive primarily to van der Waals interactions. The combined measurements of water and diiodomethane enable the determination of the surface energy of a material, broken into polar and dispersive components [35] [36].

Measurement control and data analysis were facilitated through the utilization of the KRÜSS ADVANCE software, and pertinent instrument parameters are documented in Table 2 for reference. To achieve scientific rigor, the equipment and procedures employed adhered to precise standards and methodologies, fostering reproducibility and ensuring data integrity.

Table 2
Measurement parameters

Temperature [°C]	25
Orientation	Sessile drop
Fitting method	ellipse
Baseline setting	manual
Superficial free energy to determine used models	EoS Fowkes

The measurements were conducted utilizing the EoS and Fowkes model to determine the advancing and receding contact angles.

Measurement errors in the KRÜSS DSA30 can arise from improper baseline determination, inaccurate droplet profile detection, and environmental factors such as vibrations or inconsistent lighting. Proper calibration, a stable environment, and precise operator technique – including accurate liquid dosing and surface preparation – are essential to minimize these issues. Following the manufacturer's guidelines and ensuring optimal experimental conditions can significantly enhance measurement reliability [37].

2.4.1 EoS Model

An equation of state, which characterizes the system's state based on thermodynamic variables such as pressure, temperature, volume, and particle count, was employed. In accordance with Young's equation, the relationship between the edge angle (θ), liquid surface tension (σ_l), solid-liquid interfacial tension (σ_{sl}), and solid surface tension (σ_s) is expressed as follows:

$$\sigma_s = \sigma_{sl} + \sigma_l.cos\theta \quad (8)$$

To calculate the interfacial tension (σ_{sl}), Neumann proposed the equation (9):

$$\sigma_{sl} = \sigma_l + \sigma_s - 2\sqrt{\sigma_l.\sigma_s}e^{-\beta(\sigma_l-\sigma_s)^2} \quad (9)$$

The empirically determined value of the constant β is 0.0001247 [36].

2.4.2 Fowkes Model

The Fowkes method calculates surface tension (σ_{sl}) based on surface tensions (σ_s and σ_l) and interactions between phases. The interactions are considered as the geometric mean of the dispersion part (σ^D) and polar (non-dispersion part, σ^{nD}) of surface tension, as per the relation (10):

$$\sigma_{sl} = \sigma_l + \sigma_s - 2\left(\sqrt{\sigma_l^D.\sigma_s^D} + \sqrt{\sigma_l^{nD}.\sigma_s^{nD}}\right) \quad (10)$$

The determination of solid surface tension involves two steps: first, the dispersion part is determined with a purely apolar liquid, and then the polar part is defined using at least one additional fluid containing a polar surface tension component [38].

3 Results and Discussion

3.1 Definition of Surface Tension

During the experiments, water and diiodomethane (CH_2I_2) droplets were employed to ascertain the dispersion and polar components of surface energy. The total surface energy value was determined by summing these components.

In the evaluation process, both EoS and Fowkes methods were used. Due to sample moistening or dissolution, and the absence of a well-defined baseline, the two-fluid (Fowkes) model could not be universally applied. Consequently, the evaluation differentiated between surface free energy values obtained by the two measurement methods. The single-liquid (EoS) method was employed when only evaluable images with one liquid were available. In contrast, the two-fluid (Fowkes) model was applied when high-quality images were obtained from different points with both dispersion and polar fluids.

The measurement protocol involved constant-volume droplets for various material pairs, including ABS-water, PLA-water, white epoxy resin-water, white epoxy resin-diiodomethane (CH_2I_2), gray epoxy resin-water, gray epoxy resin-diiodomethane, bronze powder-filled PLA-water and bronze powder-filled PLA-CH_2I_2.

The surfaces of pure ABS and PLA were dissolved by diiodomethane and cyclohexane, causing droplets to flow over time, rendering the method unsuitable for edge angle testing in these cases.

3.2 Surface Free Energy Measurements

Using the Krüss Advanced software, surface free energy values were calculated from edge angle measurements, employing either the EoS or Fowkes method based on the one-solution or two-solution method. It is noteworthy that a surface tension value of 34 mN/m is widely accepted as a limit for wetting during practical applications: surfaces with $\gamma < 34$ mN/m are non-wettable, while those with $\gamma > 34$ mN/m exhibit good wetting properties.

The (total) surface energy of materials is considered the sum of dispersion (γ_d) [mN/m] and polar (γ_p) [mN/m] components:

$$\gamma = \gamma_d + \gamma_p [\frac{mN}{m}] \tag{11}$$

Table 3 presents the measurement results for various materials using water and diiodomethane, providing information on the perimeter angle mean (M), left-sided edge angle, and right-sided edge angle. However, the data for diiodomethane is marked as "no stable droplet shape", indicating that these measurements were not conducted or could not be evaluated for the specified conditions. The table shows varying perimeter angle means for ABS and PLA, reflecting differences in wetting behavior. White epoxy resin consistently exhibits higher perimeter angle means compared to gray epoxy resin, suggesting differences in wetting behavior. Similar to ABS and PLA, measurements for water are available, indicating potential variations in wetting behavior.

Figure 4 displays photographs of water and diiodomethane drops on different 3D-printed surfaces during the measurement process. Tables 4 and 5 summarize the results obtained from the measurement data. Table 4 (Single-Solution Method) provides the surface energy values for each material using the single-solution method without using diiodomethane. Notably, ABS has a higher surface energy compared to PLA, while epoxy resins and bronze powder-filled PLA exhibit even higher values. In Table 5 (Two-Solution Method), the surface energy values are broken down into dispersive and polar components for each material, derived from Equations 8-10. The results indicate differences in the material's interaction with water and diiodomethane.

The results indicate that gray and white epoxy resin have the highest surface free energy. High surface energy implies a stronger adhesion tendency, potentially leading to increased friction and wear during application. Polylactic acid (PLA) has the lowest surface free energy value of 9.64 mN/m, suggesting its potential suitability for plastic-plastic friction, where lubricants do not adhere to the surface.

The addition of bronze powder to PLA increased the surface free energy value. However, both PLA and ABS have surface free energy values below the practical limit of 34 mN/m, indicating non-wettability from a lubrication perspective. The results also show that the gray epoxy resin has the highest surface free energy. Although the surface free energy values for all three materials exceed the practical limit of 34 mN/m, their polar components differ: the polar surface free energy of PLA filled with bronze powder is 1.86 mN/m, while that of resins is 11.20 and 11.26 mN/m, respectively.

For PLA filled with bronze powder, the one- and two-solution methods yielded different surface free energy values, necessitating further tests for accurate assessment.

Table 3

Measurements of tested materials with water and diiodomethane (minus the smallest and largest result)

	Measure-ment number	Water			Diiodomethan		
		Perimeter angle mean (M)°	Left sided edge angle°	Right lateral edge angle°	Perimeter angle mean (M)°	Left sided edge angle°	Right lateral edge angle°
ABS	1	88.67	86.99	90.35	no stable droplet shape		
	2	92.16	91.89	92.43	no stable droplet shape		
	3	95.42	95.19	95.65	no stable droplet shape		
PLA	1	124.13	124.43	123.83	no stable droplet shape		
	2	129.26	129.72	128.81	no stable droplet shape		
	3	130.30	130.84	129.75	no stable droplet shape		
White epoxy resin	1	75.76	74.06	77.47	63.93	58.51	69.35
	2	76.54	76.82	76.26	63.87	60.11	67.63
	3	78.67	78.81	78.52	56.39	49.26	63.52
Gray epoxy resin	1	69.00	63.39	74.60	59.36	62.22	56.50
	2	71.48	73.61	69.35	50.21	52.70	47.72
	3	71.84	70.96	72.72	45.48	36.08	54.88
Bronze powder filled	1	87.81	88.28	87.34	48.44	48.97	47.92
	2	86.43	86.10	86.76	48.17	43.92	52.41
	3	68.64	88.12	83.98	51.32	45.99	56.64

In Figure 4, each subfigure corresponds to a specific material and measurement method. For instance, Figure 4(a) and (b) depict water and diiodomethane drops on FDM 3D-printed ABS surface during the measurement using the Eos and Fowkes methods, respectively. Figure 4(c) shows a water drop residing on FDM 3D-printed PLA surface during the measurement using the Eos method. Figure 4(d) illustrate a diiodomethane drop residing on DLP 3D-printed PLA surface during the measurement using the Fowkes method. Figure 4(e) depicts a water drop residing on DLP 3D-printed white resin surface during the measurement using the Eos method. Figure 4(f) displays a diiodomethane drop residing on DLP 3D-printed white resin surface during the measurement using the Fowkes method.

	Water	Diiodomethan
ABS	**(a)** 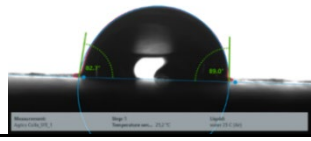	**(b)** Solved by the sample its surface
PLA	**(c)** 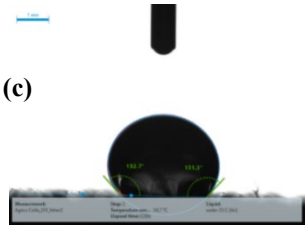	**(d)**
White epoxy resin	**(e)** 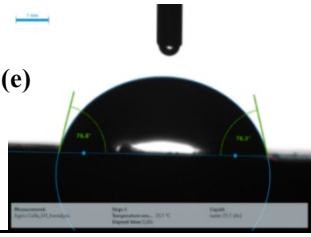	**(f)** 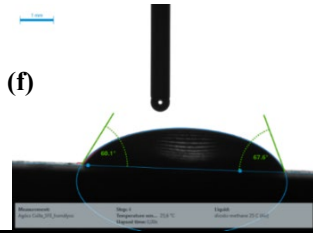
gray epoxy resin	**(g)** 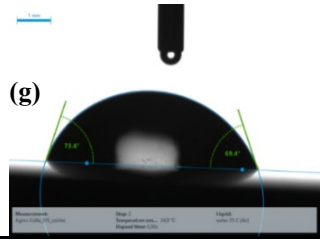	**(h)** 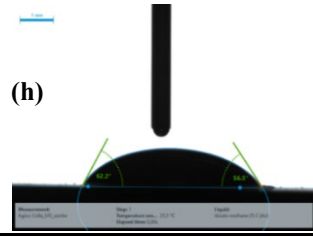
Bronze powder filled PLA	**(i)** 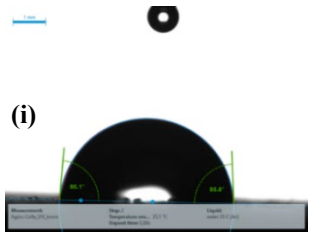	**(j)** 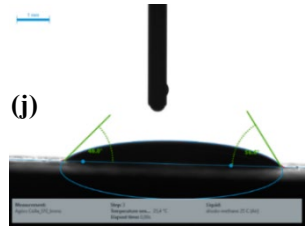

Figure 4

Photographs of water and diiodomethane drops on various 3D-printed surfaces while measuring

Figure 4(g) exhibits a water drop residing on DLP 3D-printed gray resin surface during the measurement using the Eos method. Figure 4(h) present a diiodomethane drop residing on DLP 3D-printed gray resin surface during the measurement using the Fowkes method. Figure 4(i) demonstrates a water drop residing on FDM 3D-printed bronze powder filled PLA surface during the measurement using the Eos method. Figure 4(j) depicts a diiodomethane drop residing on FDM 3D-printed bronze powder filled PLA surface during the measurement using the Fowkes method.

Table 4
Measurement results for single-solution method based on calculations with Krüss Advanced software

	ABS	**PLA**	**With bronze powder filled PLA**	**White epoxy resin**	**Gray epoxy resin**
Total surface energy $[\frac{mN}{m}]$	27.91	9.64	30.03	41.09	43.81

Table 5
Measurement results for the two-solution method based on calculations with Krüss Advanced software

	ABS	**PLA**	**With bronze powder filled PLA**	**White epoxy resin**	**Gray epoxy resin**
Dispersive ferry $[\frac{mN}{m}]$	-	-	34.66	27.04	33.33
Polar ferry $[\frac{mN}{m}]$	-	-	1.86	11.26	11.20
Complete up No. energy $[\frac{mN}{m}]$	-	-	36.52	38.30	44.53

A relatively large deviation of the measurement angles (e.g., white epoxy) can be caused by different effects, such as inadequate recognition of the shape of the drop, inadequate lighting leading to inaccurate identification of the edge of the drop, and even environmental effects (vibration, uneven lighting).

The findings indicate that the quality of raw materials exerts a lesser influence on the surface energy values of components fabricated using Digital Light Processing (DLP) compared to those produced via Fused Deposition Modeling (FDM). This discrepancy can primarily be attributed to the greater degree of micro-geometric variability inherent in FDM surfaces, which are less precisely controlled than those created through DLP. Notably, DLP technology yields consistent surface energy values across both polar and dispersive components, demonstrating its precision and reliability in maintaining uniform surface characteristics.

In terms of comparing materials effect, the surface tension increased for the FDM-printed PLA containing bronze powder compared to natural PLA. In a similar context, natural ABS displayed a much higher surface energy than natural PLA, confirming the material-specific effect on the surface tension. Such differences also matter for applications like machine elements that are frictional, where adding

something internally, like powder made of bronze, will modify adhesion properties and therefore change the resulting friction characteristics. These adjustments might even assist in reducing the "stick-slip" dynamics, a common challenge in industrial processes.

Figures 5 and 6 show how 3D printing technologies influence the surface characteristics of the measured polymeric materials. It was found that the influence of 3D printing on surface free energy (SFE) was not limited to material selection but also included variations in surface roughness. Increased roughness increases the contact area between surfaces and liquids and thus increases interaction and can increase the SFE. The type of filament (PLA, ABS, or PETG, for example) and also the printing parameters (temperature, layer height) can influence material properties, such as crystallinity, which impact SFE. Higher printing temperatures, for instance, may reduce surface roughness but could also modify the material structure, impacting its surface energy characteristics.

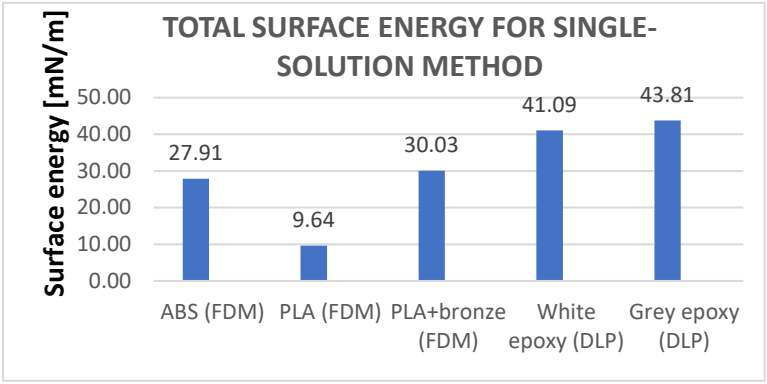

Figure 5
Comparison of 3D printing methods' influence on total surface energy for single-solution method

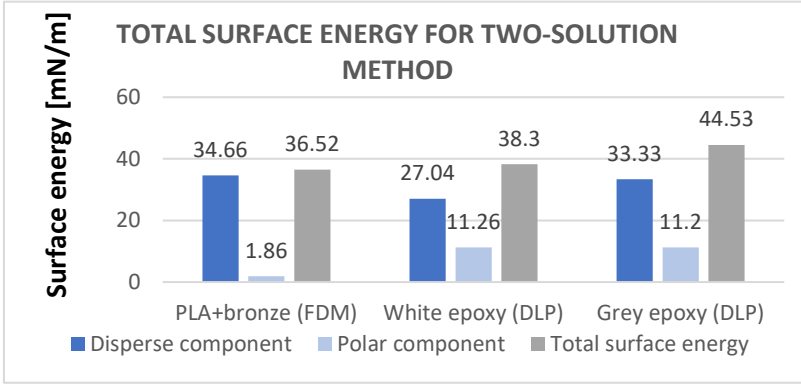

Figure 6
Comparison of 3D printing methods' effect on total surface energy for two-solution method

Post-processing techniques further contribute to these variations. Processes like polishing or plasma treatment can enhance adhesion and wettability by altering surface properties. For DLP printing, the process is followed by the UV curing which causes a hardening effect in the surface which relates a lot to the surface properties. Moreover, the way and depth of cleaning printed surfaces have a role to play, as they establish the differences influencing final surface energy. In summary, the SFE of 3D-printed materials is very sensitive to manufacturing process and post-processing techniques. These combined elements allow for the customization of surface properties needed to satisfy the needs of specific applications, especially in those requiring a high degree of control of surface interactions.

Overall, variations in perimeter angle means indicate different wetting behaviors resulting from the morphology tested, with ramifications for adhesion and surface interactions. The elevated surface energy values explain the high adhesion of epoxy resins and bronze powder-filled PLA, as evident from Tables 4 and 5. The difference between water and diiodomethane measurements of deposition may suggest that these liquids wet the tested materials differently. However, a thorough understanding of the wetting behaviors and surface energy values observed will require correlating these results to the experimental conditions and manufacturing parameters.

Conclusions

The presented work captures the complex correlations of surface tension, wetting phenomenology and adhesion that occurs with 3D-printed parts. The surface tension properties of custom and commercially available materials, including ABS, PLA, epoxy resins and PLA reinforced with bronze powder, were systematically characterized using sophisticated measuring techniques. From the results obtained, we can infer the following:

1) The analysis reveals unique surface free energy (SFE) values among various materials, where gray and white epoxy resins have higher values suggesting a greater propensity for adhesion and friction properties.

2) The findings emphasize how manufacturing processes affect the SFE dynamics, as advanced 3D printing technologies, namely, fused deposition modeling (FDM) and digital light processing (DLP), influence the SFE. The surface energy values are more consistent for DLP because DLP has more accurate microgeometry control than FDM and less surface roughness variability.

3) The SFE of the PLA with bronze is higher than that of natural PLA, while the SFE of natural ABS is higher than that of PLA. These material differences play a crucial role in enhancing industrial applications, particularly in addressing adhesion and friction challenges, such as mitigating the "stick-slip" phenomenon.

4) 3D printing significantly affects SFE through changes in surface roughness and material properties. Factors such as filament type, printing parameters (e.g., temperature, layer height), and post-processing (e.g., polishing, plasma treatment, or UV curing in DLP) can be tailored to optimize SFE for specific applications.

The findings presented herein are valid at a temperature of 25 °C. As surface tension is sensitive to temperature changes, further studies across a broader temperature range are recommended to understand the thermal effects on wetting and adhesion. This research sets the stage for tailored surface tension optimization strategies, offering the potential to enhance the performance and functionality of 3D-printed components, across a range of applications in various industries.

Acknowledgements

This research was supported by PhD Programme, the Mechanical Engineering Doctoral School, Hungarian University of Agriculture and Life Science, Gödöllő, Hungary and the Flagship Research Program of MATE (KKP 2024).

References

[1] Stalder A. F., Melchior T., Müller M., Sage D., Blu T., Unser M., "Low-bond axisymmetric drop shape analysis for surface tension and contact angle measurements of sessile drops," Colloids and Surfaces A: Physicochemical and Engineering Aspects, Vol. 364, No. 1-3, pp. 72-81, 2010

[2] Nemcsics Á., "Formation Kinetics of the Self-organized III-V-based Nanostructures Grown by Droplet Epitaxy," Acta Polytechnica Hungarica, Vol. 8, No. 4, pp. 5-21, 2011

[3] Poskus M. D., Wang T., Deng Y., Borcherding S., Atkinson J., Zervantonakis I. K., "Fabrication of 3D-printed molds for polydimethylsiloxane-based microfluidic devices using a liquid crystal display-based vat photopolymerization process: printing quality, drug response and 3D invasion cell culture assays," Microsystems & Nanoengineering, Vol. 9, No. 1, p. 140, 2023

[4] Song R., Abbasi M. S., Lee J., "Fabrication of 3D printed modular microfluidic system for generating and manipulating complex emulsion droplets," Microfluidics and Nanofluidics, Vol. 23, No. 7, p. 92, 2019

[5] Hanon M. M., Ghaly A., Zsidai L., Klébert S., "Tribological characteristics of digital light processing (DLP) 3D printed graphene/resin composite: Influence of graphene presence and process settings," Materials & Design, Vol. 218, p. 110718, 2022

[6] Hanon M. M., Zsidai L., "Comprehending the role of process parameters and filament color on the structure and tribological performance of 3D

printed PLA," Journal of Materials Research and Technology, Vol. 15, pp. 647-660, 2021

[7] Sullivan D. E., "Surface tension and contact angle of a liquid–solid interface," The Journal of Chemical Physics, Vol. 74, No. 4, pp. 2604-2615, 1981

[8] Luo Y., Pang A.-P., Lu X., "Liquid–Solid Interfaces under Dynamic Shear Flow: Recent Insights into the Interfacial Slip," Langmuir, Vol. 38, No. 15, pp. 4473-4482, 2022

[9] Truzzolillo D., Mora S., Dupas C., Cipelletti L., "Nonequilibrium Interfacial Tension in Simple and Complex Fluids," Physical Review X, Vol. 6, No. 4, p. 041057, 2016

[10] Kovalchuk N. M., Simmons M. J. H., "Surfactant-mediated wetting and spreading: Recent advances and applications," Current Opinion in Colloid & Interface Science, Vol. 51, p. 101375, 2021

[11] MacGregor-Ramiasa M. N., Vasilev K., "Questions and Answers on the Wettability of Nano-Engineered Surfaces," Advanced Materials Interfaces, Vol. 4, No. 16, 2017

[12] Bormashenko E., "Progress in understanding wetting transitions on rough surfaces," Advances in Colloid and Interface Science, Vol. 222, pp. 92-103, 2015

[13] Makkonen L., "Young's equation revisited," Journal of Physics: Condensed Matter, Vol. 28, No. 13, p. 135001, 2016

[14] Sun E. W.-H., Bourg I. C., "Molecular Dynamics Simulations of Mineral Surface Wettability by Water Versus CO_2 : Thin Films, Contact Angles, and Capillary Pressure in a Silica Nanopore," The Journal of Physical Chemistry C, Vol. 124, No. 46, pp. 25382-25395, 2020

[15] Rabinovich Y. I., Adler J. J., Esayanur M. S., Ata A., Singh R. K., Moudgil B. M., "Capillary forces between surfaces with nanoscale roughness," Advances in Colloid and Interface Science, Vol. 96, No. 1-3, pp. 213-230, 2002

[16] Comtet J., Niguès A., Kaiser V., Coasne B., Bocquet L., Siria A., "Nanoscale capillary freezing of ionic liquids confined between metallic interfaces and the role of electronic screening," Nature Materials, Vol. 16, No. 6, pp. 634-639, 2017

[17] Yaghoubi H., Foroutan M., "Molecular investigation of the wettability of rough surfaces using molecular dynamics simulation," Physical Chemistry Chemical Physics, Vol. 20, No. 34, pp. 22308-22319, 2018

[18] Mueller B., "Additive Manufacturing Technologies – Rapid Prototyping to Direct Digital Manufacturing," Assembly Automation, Vol. 32, No. 2, 2012

[19] Hanon M. M., Zsidai L., "Sliding surface structure comparison of 3D printed polymers using FDM and DLP technologies," IOP Conference Series: Materials Science and Engineering, Vol. 749, No. 1, 2020

[20] Hanon M. M., Zsidai L., "Tribological and mechanical properties investigation of 3D printed polymers using DLP technique," 2020, p. 020205

[21] Hanon M. M., Ghaly A., Zsidai L., Szakál Z., Szabó I., Kátai L., "Investigations of the Mechanical Properties of DLP 3D Printed Graphene/Resin Composites," Acta Polytechnica Hungarica, Vol. 18, No. 8, pp. 143-161, 2021

[22] Fatima Faidallah R., M. Hanon M., Szakál Z., Oldal I., "Study of the Mechanical Characteristics of Sandwich Structures FDM 3D-printed," Acta Polytechnica Hungarica, Vol. 20, No. 6, pp. 7-26, 2023

[23] Kónya G., Ficzere P., "The Effect of Layer Thickness and Orientation of 3D Printed Workpieces, on The Micro- and Macrogeometric properties of Turned Parts," Acta Polytechnica Hungarica, Vol. 21, No. 2, pp. 231-250, 2024

[24] Hashemi Sanatgar R., Campagne C., Nierstrasz V., "Investigation of the adhesion properties of direct 3D printing of polymers and nanocomposites on textiles: Effect of FDM printing process parameters," Applied Surface Science, Vol. 403, pp. 551-563, 2017

[25] Huang J., Qi L., Luo J., Hou X., "Insights into the impact and solidification of metal droplets in ground-based investigation of droplet deposition 3D printing under microgravity," Applied Thermal Engineering, Vol. 183, p. 116176, 2021

[26] Özenç M., Tezel T., Kovan V., "Investigation into impact properties of adhesively bonded 3D printed polymers," International Journal of Adhesion and Adhesives, Vol. 118, p. 103222, 2022

[27] Zeng H., Ed., Polymer Adhesion, Friction, and Lubrication. 2013

[28] Skalon M., Meier B., Leitner T., Arneitz S., Amancio-Filho S. T., Sommitsch C., "Reuse of Ti6Al4V Powder and Its Impact on Surface Tension, Melt Pool Behavior and Mechanical Properties of Additively Manufactured Components," Materials 2021, Vol. 14, No. 5, p. 1251, 2021

[29] Gao J., Rong W., Gao P., Wang L., Sun L., "A programmable 3D printing method for magnetically driven micro soft robots based on surface tension," Journal of Micromechanics and Microengineering, Vol. 31, No. 8, p. 085006, 2021

[30] Chan K. P., He F., Atwah A. A., Khan M., "Experimental investigation of self-cleaning behavior of 3D-printed textile fabrics with various printing parameters," Polymer Testing, Vol. 119, pp. 107941, 2023

[31] Kalkandelen C., Ozbek B., Ergul N. M., Akyol S., Moukbil Y., Oktar F. N., Ekren N., Kilic O., Kilic B., Gunduz O., "Effect of temperature, viscosity and surface tension on gelatin structures produced by modified 3D printer," IOP Conference Series: Materials Science and Engineering, Vol. 293, No. 1, pp. 012001, 2017

[32] Eötvös R., "Ueber den Zusammenhang der Oberflächenspannung der Flüssigkeiten mit ihrem Molecularvolumen," Annalen der Physik, Vol. 263, No. 3, pp. 448-459, 1886

[33] Tyowua A. T., Yiase S. G., "Contact Angle Hysteresis – Advantages and Disadvantages: A Critical Review," Progress in Adhesion and Adhesives, Volume 6, pp. 47-67, 2021

[34] Benilov E. S., "Dependence of the surface tension and contact angle on the temperature, as described by the diffuse-interface model," Physical Review E, Vol. 101, No. 4, pp. 042803, 2020

[35] Israelachvili J. N., Intermolecular and Surface Forces, 3rd Edition. University of California, Santa Barbara, California, USA, 2011

[36] Kwok D. Y., Neumann A. W., "Contact angle interpretation in terms of solid surface tension," Colloids and Surfaces A: Physicochemical and Engineering Aspects, Vol. 161, No. 1, pp. 31-48, 2000

[37] Kwok D. Y., Neumann A. W., "Contact angle measurement and contact angle interpretation," Advances in Colloid and Interface Science, Vol. 81, No. 3, pp. 167-249, 1999

[38] Law K.-Y., Zhao H., "Determination of Solid Surface Tension by Contact Angle," Surface Wetting, pp. 135-148, 2016